RSC Advances

PAPER

View Article Online
View Journal | View Issue

Cite this: *RSC Adv.*, 2023, **13**, 34852

Synthesis and evaluation of photophysical, electrochemical, and ROS generation properties of new chalcogen-naphthoquinones-1,2,3-triazole hybrids†

Luana S. Gomes,[a] Érica O. Costa,[a] Thuany G. Duarte,[a] Mateus H. Köhler,[b] Bruna M. Rodrigues,[c] Vitor F. Ferreira,[d] Fernando de C. da Silva,[e] Bernardo A. Iglesias *[c] and Vanessa Nascimento *[a]

Received 13th October 2023
Accepted 20th November 2023

DOI: 10.1039/d3ra06977j

rsc.li/rsc-advances

This study presents a comprehensive analysis encompassing the synthesis, structural elucidation, photophysical behavior, and electrochemical properties of a novel series of chalcogen-naphthoquinone-1,2,3-triazole hybrids. Employing a meticulously designed protocol, the synthesis of these hybrids, denoted as **11a–j**, was achieved with remarkable efficiency (yielding up to 81%). This synthesis used a regioselective copper-catalyzed azide–alkyne cycloaddition reaction (CuAAC). Furthermore, a detailed investigation into the photophysical characteristics, TDDFT calculations, electrochemical profiles, and photobiological attributes of compounds **11a–j** was conducted. This exploration aimed to unravel insights into the excited state behaviors of these molecules, as well as their redox properties. Such insights are crucial for future applications of these derivatives in diverse biological assays.

Introduction

A molecular hybrid is created through the fusion of two or more pharmacologically active groups in order to produce a new chemical entity that carries over significant characteristics from the parent molecules with the aim of optimizing their pharmaceutical properties.[1] This strategy has the potential to produce chemical libraries with high structural information levels.[2] In this way, according to the interests of our research group, in this work we will report the synthesis and electrochemical/photophysical studies of unprecedent molecular hybrids containing quinones, organochalcogens and triazoles.

In this context, quinones, which constitute a broad and varied family of naturally occurring metabolites, are extensively employed as building blocks for creating hybrids with diverse functional profiles.[3] The interest in these substances has grown in recent years due to their biooxidation–reduction properties and ability to catalyze biological electron transfer processes, mainly in numerous pharmaceutical research studies.[4,5] Therefore, depending on the system, quinones can act as antioxidants and protect cells from reactive oxygen species (ROS) or as cytotoxic agents, generating such reactive species, which are important in processes involving certain diseases, such as cancer, degenerative diseases, and tropical diseases, among others (Fig. 1).[6,7]

In addition, naphthoquinones have photophysical capabilities that allow them to absorb and emit light in a highly efficient manner due to their conjugated structural characteristics.[8] The significance of these compounds stems from their activity as fluorophores, which are widely employed in biomedical applications as fluorescent markers in studies of living cells and tissues, as well as in diagnostic tests and disease monitoring.[9] Furthermore, because of their ability to efficiently transport

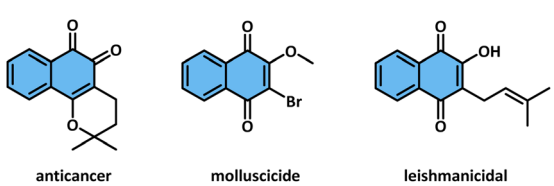

Fig. 1 Pharmacologically active naphthoquinone compounds.

[a]*Department of Chemistry, SupraSelen Laboratory, Federal University Fluminense, Institute of Chemistry, Campus do Valonguinho, Niterói, 24020-141, RJ, Brazil. E-mail: nascimentovanessa@id.uff.br*

[b]*Department of Physics, Federal University of Santa Maria, Santa Maria, 97105-900, RS, Brazil*

[c]*Department of Chemistry, Bioinorganic and Porphyrin Materials Laboratory, Federal University of Santa Maria, Santa Maria, 97105-900, RS, Brazil. E-mail: bernardopgq@gmail.com*

[d]*Faculty of Pharmacy, Department of Pharmaceutical Technology, Niterói, 24241-000, RJ, Brazil*

[e]*Laboratório de Síntese Orgânica Aplicada (LabSOA), Institute of Chemistry, Universidade Federal Fluminense, Niterói, 24020-141, RJ, Brazil*

† Electronic supplementary information (ESI) available: NMR spectra [^{1}H, ^{13}C and HRMS (APPI+)]. See DOI: https://doi.org/10.1039/d3ra06977j

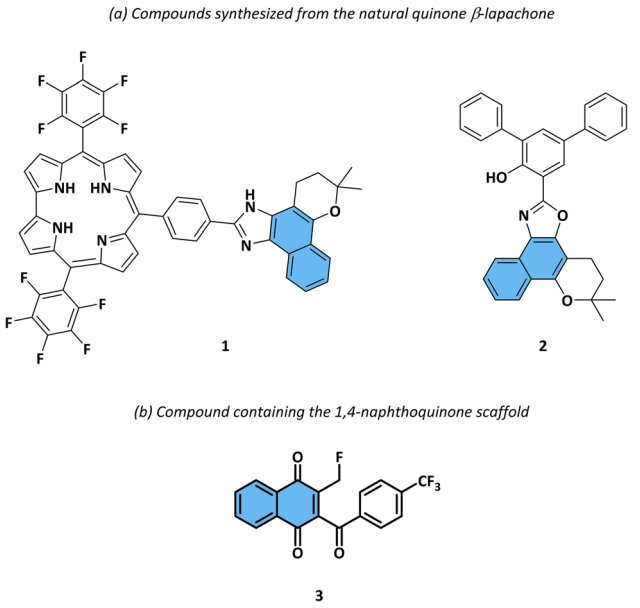

Fig. 2 (a) A compound originating from naphthoquinones featuring heterocyclic rings and (b) encompassing the 1,4-naphthoquinone framework, both demonstrating photophysical properties.

energy, they are useful in the development of optoelectronic devices, such as light emitting diodes (LEDs) and solar cells, which are driving breakthroughs in clean energy and energy efficiency.[10]

In the context, recently Rodrigues *et al.*[11] focused on the synthesis, characterization, and photophysical evaluation of a novel derivatives from β-lapachone **1**. This quinoid compound demonstrated the ability to yield remarkably fluorescent heterocyclic compounds, such as lapimidazoles (Fig. 2a). This research shed light on the potential of utilizing β-lapachone as a precursor to develop fluorescent molecules with diverse applications in the fields of chemistry and materials science.[12] Another study, published by Dias *et al.*,[13] describes a strategy for the synthesis of four new oxazole naphtoquinone derivatives **2** with a tendency to intramolecular proton transfer in the excited fluorescent state (ESIPT). This class of compounds derived from lapachol and opening the way for a new class of bioprobes (Fig. 2a). Furthermore, in a study conducted by Trometer *et al.*[14] the authors concentrated on adding fluorine into the 2-methyl group of 1,4-naphthoquinone, which resulted in considerable alterations in the compound's redox characteristics, making it highly oxidizing and photoreactive. Thus, the compound **3** exhibit emission properties in the visible region, making it effective as a fluorescent probe to monitor protein alkylation processes and oxidation state in living cells, such as BY-2 tobacco cells, which demonstrated high fluorescence emission (Fig. 2b).

Additionally, organochalcogens, especially organoselenium compounds, have been widely studied due to the large number of synthetic and biological applications. These molecules have been described as antioxidants or pro-oxidants, depending on their environment.[15]

In the last decades, chalcogens (O, S, Se, and Te) have received great attention for applications in materials.[16,17] Recently, Silveira and collaborators[18] synthesized a series of organoselenium compounds with photophysical properties UV-Vis and steady-state emission fluorescence. In the UV-Vis study, for example, all derivatives revealed transition bands in the ultraviolet and visible window between 270 and 450 nm. Electronic transitions were also seen, which may be connected to $\pi \rightarrow \pi^*$ and $n \rightarrow \pi^*$ transitions, and modest changes in the spectra were observed when the polarity of the solvent or substituent was changed in all compounds (Scheme 1a).

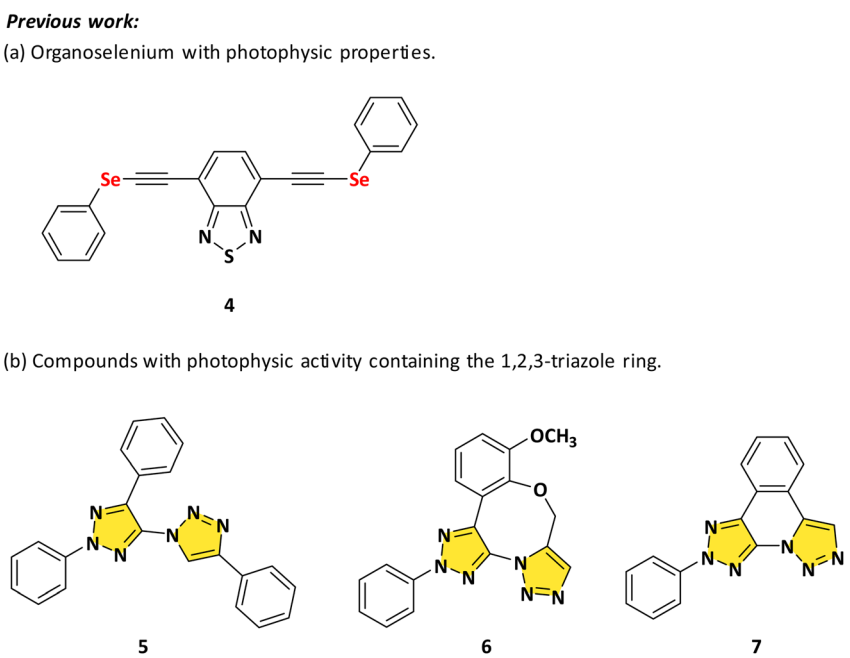

Scheme 1 Compounds containing selenium and the 1,2,3-triazole ring and their photophysical activities.

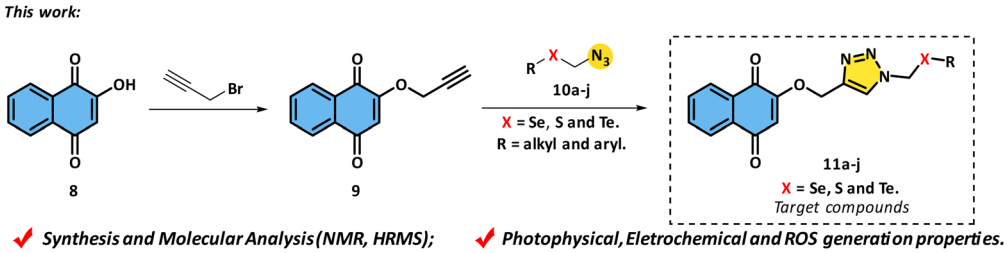

Scheme 2 General synthetic route of chalcogen-naphthoquinones-1,2,3-triazoles.

Another prominent scaffold is the 1,2,3-triazole nucleus who have a wide range of applications, including explosives, agrochemicals, and mostly medicines.[19] Due to the biological activities associated with the 1,2,3-triazole ring, it is used as an important linker in new pharmacologically active molecules and showed properties such as anti-inflammatory,[20] anticonvulsant,[21] antioxidant,[22] antibacterial,[23] antiviral,[24] antifungal,[25] anti-*T. cruzi* (*Trypanosoma cruzi*),[26] antitubercular,[27] anticancer,[28] anti-HIV (Human Immunodeficiency Virus),[29] and anti-Alzheimer.[30] Moreover, the distinct electronic structure of this ring, along with its polydentate nature, allows it to effectively bind to metal ions and analytes, making it an ideal choice for chemosensors used in qualitative and quantitative studies.[31] Safronov *et al.*,[32] for example, studied the photophysical properties of three types of 1,2,3-triazoles. The compounds showed strong UV absorption with high molar extinction coefficients (up to 73 900 M^{-1} cm^{-1}), blue emission at 350–385 nm **5–6** and 399–435 nm **7** with moderate quantum yields (up to 42.2%), and relatively long fluorescence lifetimes (from 1.05 to 4.53 ns). Therefore, these triazoles have important characteristics because they can be used as high-performance antennas or as blue components in the development of OLEDs, as well as in the design and construction of high-efficiency light-harvesting systems (LHSs) using fluorescence (Scheme 1b).

Hence, the combination of organochalcogens, naphthoquinones, and 1,2,3-triazoles to generate novel potent hybrids, replete with distinctive and multifaceted attributes capable of showcasing intriguing photophysical properties, stands as a promising and innovative perspective.[33] The union of these nuclei can provide a wide range of photophysical properties which is required for the development of advanced devices, such as highly sensitive optical sensors, efficient organic light emitting diodes (OLEDs), and energy storage and conversion systems. Investing in the synthesis of these new organic compounds represents a promising scientific and technological strategy for developing sophisticated and unique materials with major practical applications in a variety of fields (Scheme 2).

Results and discussion

The propargylation of commercial lawsone **8** is the first step in the proposed synthetic route. Rocha *et al.*[34] described this reaction using propargyl bromide, potassium carbonate, and DMF (dimethylformamide) as solvents for 24 hours at 60 °C with a yield of 60% (Scheme 3a). In parallel, the synthesis of azide selenium derivatives occurred from chloride species and was carried out using the Huang and Duan[35] method of dichloromethane substitution reactions with the arylchalcogenolate anion. This anion was formed by reacting the respective diorganoyl dichalcogenides **12a–j** with the reducing agent $NaBH_4$ in the presence of ethanol. The reaction was kept under reflux for 12 hours, and the corresponding chlorides **13a–j** were obtained in good yields (80–92%, Scheme 3b). The next step was carried out in the presence of sodium azide in CH_3CN, using crown ether 18-crown-6, yielding the respective azides **10a–j** in 87–95% yields (Scheme 3c).[36] It is worth mentioning that diorganoyl diselenides with very strong electron withdrawing groups were also tested, such as –F, $–CF_3$, and $–NO_2$, but these derivatives did not produce the desired product, instead forming only the corresponding diselenide as a decomposition product. When other chalcogens, such as sulfur and tellurium, were used, the yield remained close to selenium derivatives, both in the chlorinated intermediate and azide formation steps.

Finally, the new target series of chalcogen molecules were synthesized using a 1,3-dipolar cycloaddition reaction catalyzed by Cu(I)[37] and the protocol is based on the work developed by Sharpless and collaborators.[38] In this work, the reaction occurs between alkyne **9** and chalcogen-azides **10a–j**. The reaction was carried in a $CH_2Cl_2 : H_2O$ (1 : 1) solution for 24 hours at room temperature using $CuSO_4 \cdot 5H_2O$ and sodium ascorbate; as a result, it was possible to obtain compound **11a** in 70% yield (Scheme 4).

In order to study the effects of substituents in the organochalcogen moiety, donor and acceptor electrons groups were inserted into the final molecule. Furthermore, alkyl and heterocyclic ring groups have been applied in the aim to obtain the expected compounds. Using this protocol, it was possible to achieve a yield of 63% from the electron withdrawing group (EWG) represented by 4-Cl (compound **11b**), while the electron donating groups (EDG), represented by 4-CH_3, 4-OCH_3, and 1,2,5-CH_3 (**11c–e**), yielded 60%, 61%, and 64%, respectively. The compound containing an alkyl group (**11f**) yielded 53%, while the heterocyclic ring derivative (**11g**) was obtained with a 68% yield. A naphthyl group was also investigated, and compound **11h**, as well as the standard compound **11a**, were obtained in 70% yield. With these results, it was possible to conclude that electronic effects should not be considered at this time. In order to investigate the effect of the chalcogen atom, compounds **11i**, containing sulfur, and **11j**, containing tellurium, were obtained with yields of 81% and 30%, respectively (Scheme 4).

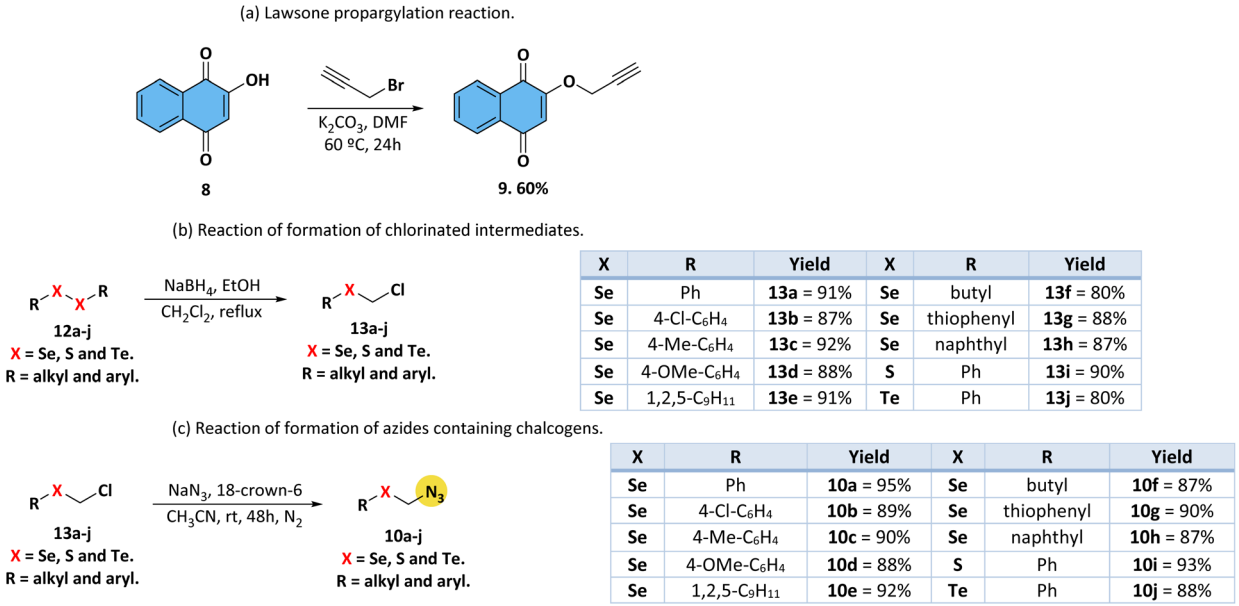

X	R	Yield	X	R	Yield
Se	Ph	**13a** = 91%	Se	butyl	**13f** = 80%
Se	4-Cl-C_6H_4	**13b** = 87%	Se	thiophenyl	**13g** = 88%
Se	4-Me-C_6H_4	**13c** = 92%	Se	naphthyl	**13h** = 87%
Se	4-OMe-C_6H_4	**13d** = 88%	S	Ph	**13i** = 90%
Se	1,2,5-C_9H_{11}	**13e** = 91%	Te	Ph	**13j** = 80%

X	R	Yield	X	R	Yield
Se	Ph	**10a** = 95%	Se	butyl	**10f** = 87%
Se	4-Cl-C_6H_4	**10b** = 89%	Se	thiophenyl	**10g** = 90%
Se	4-Me-C_6H_4	**10c** = 90%	Se	naphthyl	**10h** = 87%
Se	4-OMe-C_6H_4	**10d** = 88%	S	Ph	**10i** = 93%
Se	1,2,5-C_9H_{11}	**10e** = 92%	Te	Ph	**10j** = 88%

Scheme 3 (a) Synthesis of propargylated lawsone **9**; (b) synthesis of chlorinated intermediates **13a–j**; (c) synthesis of azides **10a–j**.

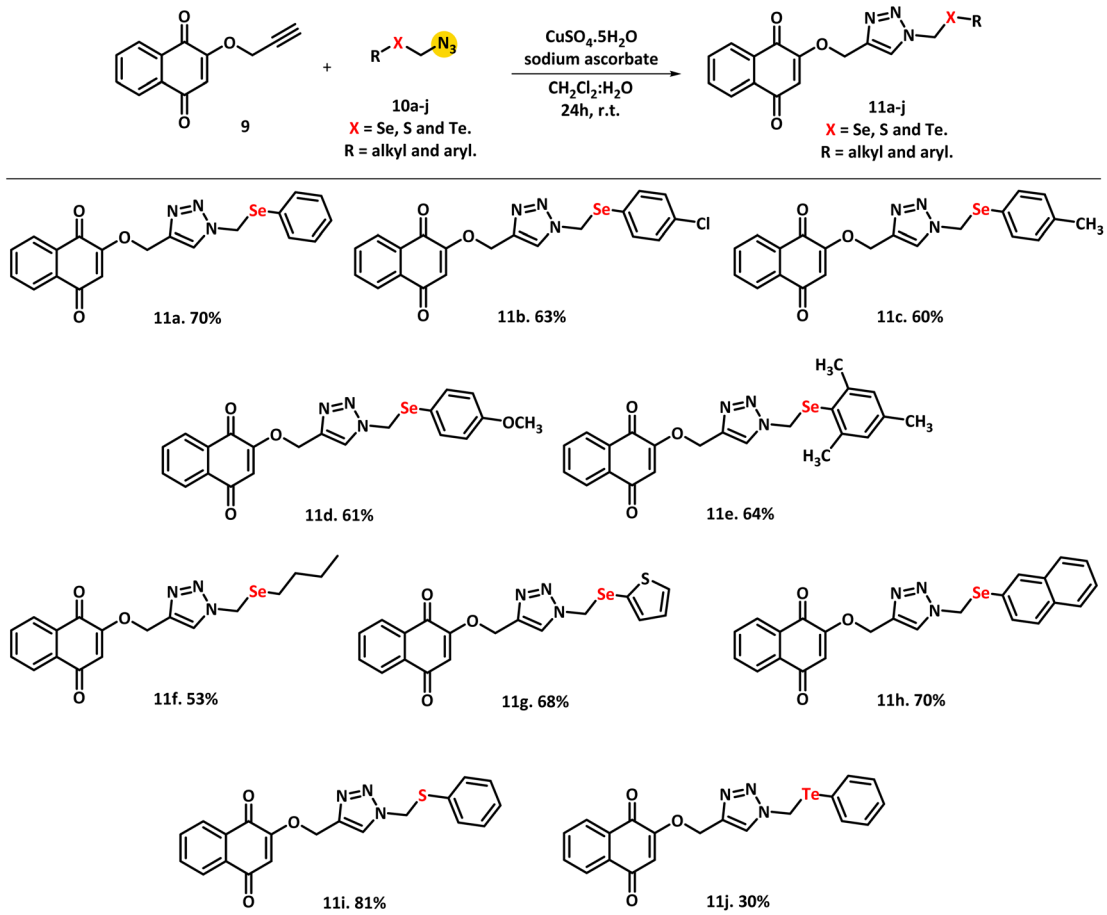

Scheme 4 Synthesis of chalcogen-naphthoquinones-1,2,3-triazoles **11a–j**.

The ^1H and ^{13}C NMR spectroscopies were used to characterize this unique series of ten compounds formed by the hybridization of organochalcogens and naphthoquinone and linked by the triazole ring. Specifically, the ^1H NMR analysis of compound **11a** revealed distinct chemical shifts, elucidating the configuration of hydrogens in the lawsone quinonoid ring and

the aromatic ring bonded to selenium. The couplings between these hydrogens were confirmed through two-dimensional COSY homocorrelation spectrum (Fig. S32 – ESI section†). Additionally, the ^{13}C NMR spectrum provided crucial information about the carbon atoms involved in the hybridization. The comprehensive explanation and visual representation can be found in the ESI (Fig. S30†), which improves understanding of this novel molecular series.

Absorption and emission properties

The UV-vis absorption and steady-state fluorescence emission spectra of compounds **11a–j** in DCM (dichloromethane), ACN (acetonitrile) and DMSO (dimethyl sulfoxide) are recorded and the photophysical parameters are listed in Table 1. As an example, Fig. 3 lists the comparative spectra between derivatives with different chalcogens (**11a** – Se, **11i** – S and **11j** – Te). The UV-vis absorption spectra of all derivatives are listed in the in the ESI (Fig. S62–S64†).

All derivatives showed transition bands located in the ultraviolet range, around 250–400 nm. The high energy electronic transitions, which can be related to $\pi \rightarrow \pi^*$-type transitions, are observed, and no significant shift was observed when changing the solvent polarity (Table 1). The broad transition band at low energies, which can be related to $n \rightarrow \pi^*$ and charge-transfer (CT) contributions, was assigned to a combination of the carbonyl and the quinone electronic system (Table 1). A similar behavior is also observed in the other solvents studied, such as ACN and DMSO. No change was detected with changing solvent polarity.

In regards to solution fluorescence emission spectra, derivatives **11a–j** has emissions in the region between violet and blue. As an example, and in comparative terms, the emission spectra of compounds **11a**, **11i**, and **11j** in the studied three solvents are shown in Fig. 4. These spectra were collected after excitation of the lowest energy band. The fluorescence emission spectra of all derivatives are listed in the ESI section (Fig. S65–S67†).

In general, the variation in the substituent group in the triazole moiety did not have a significant impact on the emission energies or intensities. Low to moderate fluorescence quantum yield (QY) values were observed for the compounds, with the

Table 1 Photophysical data of compounds **11a–j**

Compound	λ_{abs},[a] nm (ε; M^{-1} cm^{-1})	λ_{em},[b] nm (QY, %)	SS[c] (nm cm^{-1})
DCM			
11a	273 (16 110), 280 (15 780), 334 (2940)	398 (4.0)	64/4815
11b	273 (18 085), 281 (17 730), 333 (3290)	401 (2.0)	68/5090
11c	273 (17 970), 281 (17 730), 331 (3350)	400 (3.0)	69/5210
11d	273 (15 430), 281 (15 020), 332 (2730)	400 (3.5)	68/5120
11e	273 (16 540), 280 (16 140), 332 (3300)	399 (3.0)	67/5060
11f	272 (17 070), 280 (16 795), 332 (3370)	400 (2.0)	68/5210
11g	273 (20 760), 280 (20 660), 332 (4530)	408 (3.0)	76/5610
11h	274 (17 960), 280 (18 205), 302 (5560)	408 (3.0)	106/8600
11i	272 (16 340), 280 (15 885), 334 (3100)	408 (6.0)	74/5430
11j	271 (13 435), 280 (12 320), 326 (3630)	465 (4.0)	139/9170
ACN			
11a	272 (13 330), 278 (12 970), 330 (2380)	456 (2.0)	126/8370
11b	272 (16 120), 278 (15 870), 330 (2670)	447 (1.0)	117/7930
11c	272 (17 540), 278 (17 150), 330 (3075)	414 (1.0)	84/6150
11d	272 (16 570), 278 (16 290), 330 (2705)	481 (<1.0)	151/9515
11e	272 (17 570), 278 (17 190), 330 (3465)	—	—
11f	272 (19 400), 278 (19 070), 330 (3785)	418 (23.0)	88/6380
11g	272 (15 230), 278 (14 890), 329 (2855)	504 (6.0)	175/10 550
11h	272 (14 200), 278 (14 495), 300 (4645)	526 (<1.0)	226/14 320
11i	272 (19 080), 278 (18 360), 331 (3565)	422 (19.0)	91/6515
11j	270 (16 930), 278 (15 970), 325 (4745)	520 (6.0)	195/11 540
DMSO			
11a	275 (16 270), 331 (3960)	442 (24.0)	111/7590
11b	275 (15 970), 331 (3405)	440 (29.0)	109/7485
11c	275 (17 840), 331 (3960)	441 (19.0)	110/7535
11d	276 (17 460), 329 (3950)	444 (21.0)	115/7870
11e	276 (19 525), 332 (4585)	435 (17.0)	103/7130
11f	275 (20 045), 331 (5030)	443 (26.0)	112/7640
11g	276 (14 940), 330 (3700)	452 (39.0)	122/8180
11h	278 (17 205), 305 (8110)	433 (30.0)	128/9690
11i	274 (17 905), 331 (4225)	449 (28.0)	118/7940
11j	272 (14 140), 329 (4955)	502 (8.0)	173/10 475

[a] Concentration at 50 μM. [b] Concentration at 5.0 μM, using DPA in chloroform as standard (QY = 65%). [c] Stokes shifts (SS) = $(1/abs \times 10^{-7}) - (1/Em \times 10^{-7})$ cm^{-1}.

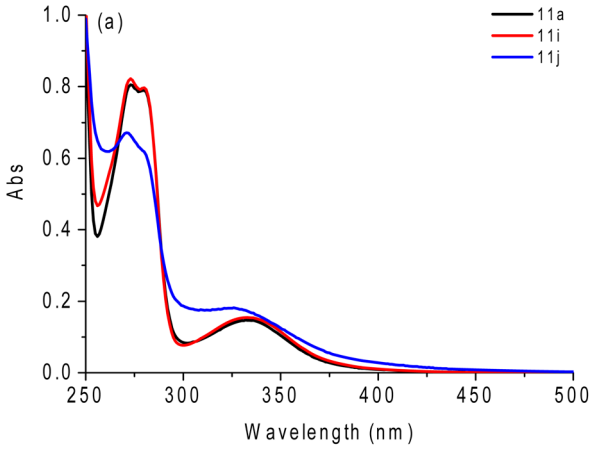

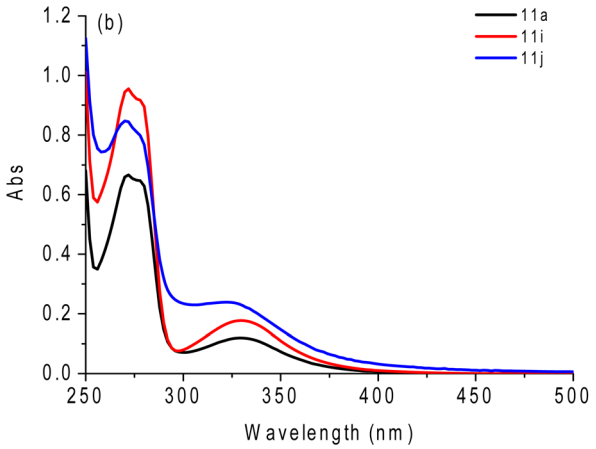

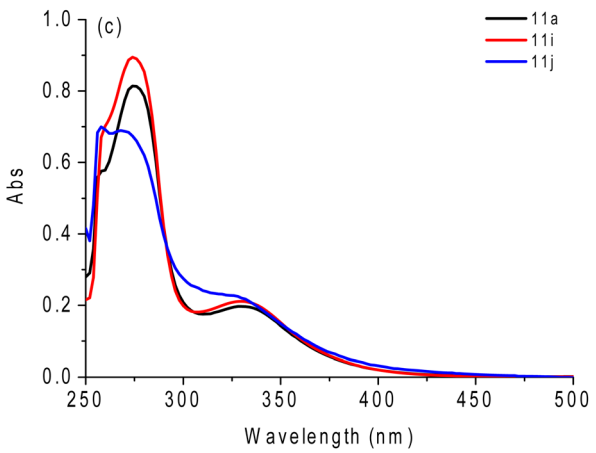

Fig. 3 Comparative absorption UV-vis spectra (concentration at 50 μM) of compounds **11a** (Se atom), **11i** (S atom) and **11j** (Te atom) in (a) DCM, (b) ACN and (c) DMSO, respectively.

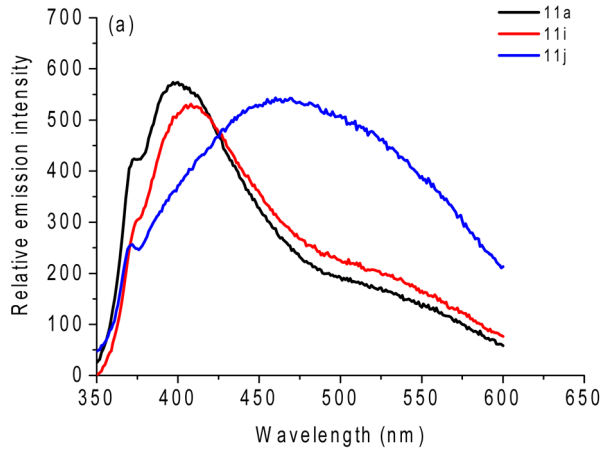

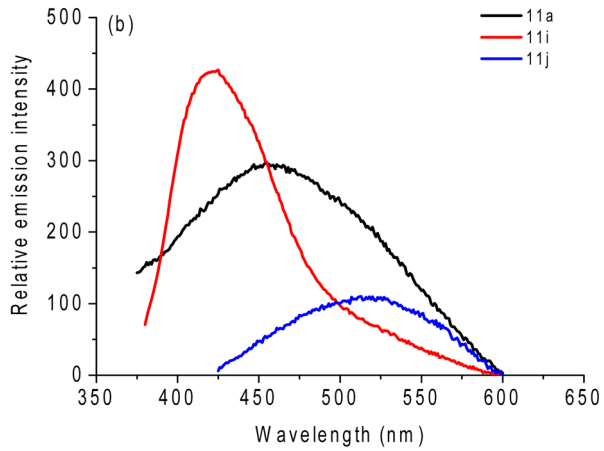

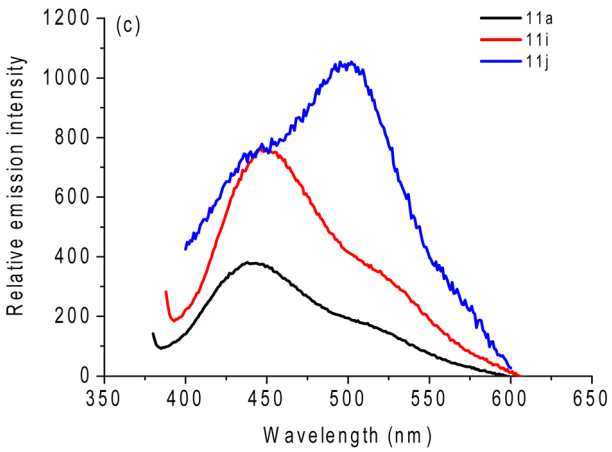

Fig. 4 Comparative steady-state fluorescence emission spectra (concentration at 5.0 μM) of compounds **11a** (Se atom), **11i** (S atom) and **11j** (Te atom) in (a) DCM, (b) ACN and (c) DMSO, respectively. The compounds were excited in the higher energy transition band.

highest values found in the DMSO solution (Table 1). Higher QY values in more polar solvents may indicate greater stabilization of excited state resonance structures by dipole–dipole interactions with surrounding solvent molecules. As in the case of the absorbance spectra, no significant differences are observed between the studied solvents (Table 1). Moderate to large Stokes shifts (SS) were observed in all compounds studied, mainly in the ACN and DMSO solutions, and can be attributed to the charge transfer state existing in these structures (Table 1).

Also, no significant change is observed depending on the chalcogen inserted, with Se derivatives having similar photophysical properties according to the literature.[39]

TDDFT analysis (time-dependent density functional theory)

Theoretical calculations by TDDFT were conducted to better elucidate the electronic nature of the studied derivatives. This way, Fig. S68 in the ESI section† shows the TDDFT optical absorption for all of the compounds in DMSO. The data were obtained at the ground state equilibrium geometry for each compound.[40] Many peaks are present in the UV region, while some optical transitions are observed in the 300–350 nm range. These results are in accordance with the experimental absorption spectra found in Fig. 3. We noticed that there was a red-shift for all optical transitions when a tellurium atom was added to the structure (compound **11j**), which indicates an interference of the heavier Te atom with the optical transitions taking place in the studied compounds.

To elucidate the optical transitions predicted by the TDDFT calculations, we show the natural transition orbitals (NTOs) associated with the larger wavelengths (330–350 nm) of the related compounds in Fig. 5. The NTOs account for a linear transformation that uses contributions from different states, so the HOMO (Highest Occupied Molecular Orbital) and LUMO (Least Unoccupied Molecular Orbital) represent an averaged transition. A careful analysis of the NTOs indicates transitions between π-orbitals at the naphthoquinone moiety; however, we observed that there are some differences in the transitions associated with the 330–350 nm peaks. For instance, in the transitions for **11a**, **11g**, and **11i**, there is a strong participation of the triazole unit on the HOMO states, while that is not observed in the other compounds. Interestingly, the tellurium

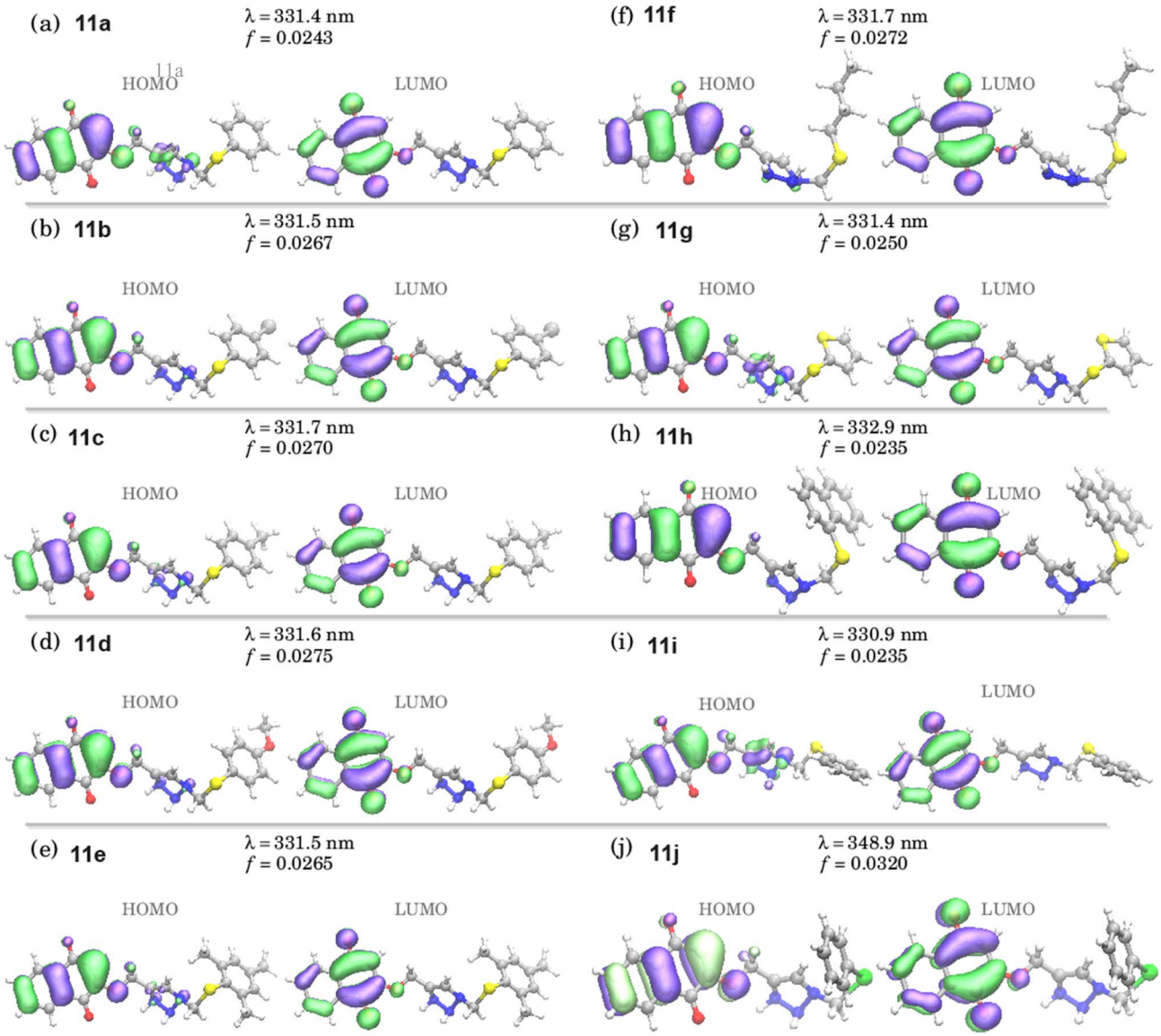

Fig. 5 NTO analysis of studied derivatives **11a–j** by TDDFT in DMSO solution.

Table 2 Redox potentials of compounds **11a–j** in DCM solution (*E versus* SHE)

Compound	E_{red1} (V)	E_{red2} (V)	E_{ox1} (V)	E_{ox2} (V)	E_{HOMO}[c] (eV)	E_{LUMO}[d] (eV)	ΔE[e] (eV)
11a	−0.87[a]	−1.34[a]	+0.76[b]	+1.70[b]	−5.16	−3.53	1.63
11b	−0.86[a]	−1.40[a]	+0.76[b]	+1.72[b]	−5.16	−3.54	1.62
11c	−0.80[a]	−1.37[a]	+0.90[b]	+1.66[b]	−5.30	−3.60	1.70
11d	−0.68[a]	−1.20[a]	+0.95[b]	+1.64[b]	−5.35	−3.72	1.63
11e	−0.73[a]	−1.30[a]	+0.92[b]	+1.84[b]	−5.32	−3.67	1.65
11f	−0.71[a]	−1.22[a]	+0.94[b]	+1.94[b]	−5.34	−3.69	1.65
11g	−0.77[a]	−1.37[a]	+0.88[b]	+1.63[b]	−5.28	−3.63	1.65
11h	−0.70[a]	−1.33[a]	+0.95[b]	+1.70[b]	−5.35	−3.70	1.65
11i	−0.85[a]	−1.37[a]	+0.78[b]	+1.86[b]	−5.18	−3.55	1.63
11j	−0.65[a]	−1.27[a]	+0.94[b]	+1.46[b]	−5.86	−3.75	2.11

[a] E_{pc} = cathodic peak. [b] E_{pa} = anodic peak. [c] $E_{HOMO} = -[4.4 + E_{ox1}$ (*versus* SHE)] eV. [d] $E_{LUMO} = -[4.4 + E_{red1}$ (*versus* SHE)] eV. [e] $\Delta E = E_{LUMO} - E_{HOMO}$.

derivative **11j** is the one that showed wavelengths and oscillator strengths for the S0 → S1 that differ from the values obtained for the other molecules.

Electrochemical analysis

Electrochemical analysis by cyclic voltammetry (CV) measurements was performed and a three-electrode system was used, consisting of a glassy carbon as the working electrode, a platinum wire as an auxiliary electrode, and a platinum wire as a pseudo-reference electrode (ferrocene was used as the internal standard; Fc/Fc^+ couple). All of the electrochemical experiments were carried out under an argon atmosphere at room temperature using a dry DCM solution of compounds **11a–j** containing 0.1 M tetrabutylammonium hexafluorophosphate ($TBAPF_6$) as the supporting electrode. All CV plots of studied derivatives are listed in the ESI section (Fig. S69†).

In general, the CVs of the derivatives displayed two irreversible oxidation peaks (E_{pa}) between +0.70 to +2.00 V and two irreversible reduction peaks (E_{pc}) between −0.60 to −1.40 V, respectively (Table 2). In the anodic region, the observed processes can involve the formation of an intermediate radical cation species in an aerobic environment, rapidly followed by a reaction with molecular oxygen to form a chalcogenoxide species (S=O, Se=O, or Te=O), according to the literature.[41,42] In the cathodic region, derivatives exhibit an irreversible reduction redox process, which can likely be assigned to the anion and di-anion radical species in the quinone moiety (Table 2).

According to Fig. 6, we can observe the comparison and relationship of potentials and energies for derivatives with different chalcogens (**11a**, **11i**, and **11j**). Derivatives containing S and Se atoms (**11a** and **11i**) were similar in terms of redox potentials,[43] with only the Te derivative (**11j**) having atypical values of redox potentials. This fact can be attributed to a change in the electronic conjugation of the molecule, disfavoring oxidation processes, making it more difficult to form a radical cation species in solution.

ROS generation assays

Compounds that have the ability to generate ROS are of great importance for biological processes and the ability of

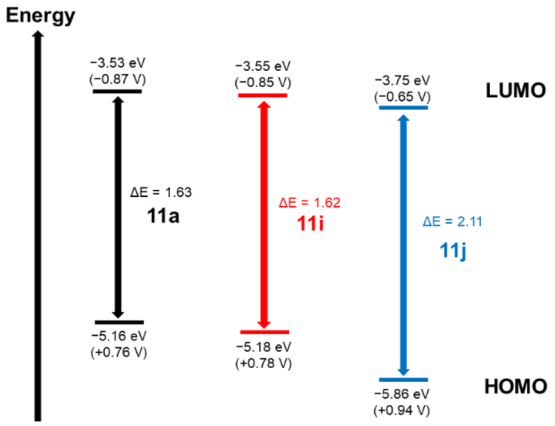

Fig. 6 Comparative redox potentials (*versus* SHE) by HOMO and LUMO levels (in eV) determined by cyclic voltammetry analysis of compounds **11a**, **11i** and **11j** in DCM solution using $TBAPF_6$ as the supporting electrolyte.

derivatives **11a–j** to generate singlet oxygen ($^1O_2$) and superoxide radicals ($O_2^{\bullet-}$). The $^1O_2$ generation was conducted from the DPBF (1,3-diphenylisobenzofuran) quencher test in DMSO, and the values of the DPBF photooxidation constants (k_{po}) and the quantum yield of singlet oxygen generation (Φ_Δ) are shown in Table 3. All UV-vis spectra of DPBF photooxidation in the presence of each compound are listed in the ESI (Fig. S70–S79†).

In general, the compounds generate $^1O_2$ with low to moderate yields, especially compounds **11c** (CH_3) and **11d** (OCH_3), which are the best singlet oxygen generators. Comparing the different chalcogen atoms in compounds **11a** (Se), **11i** (S), and **11j** (Te), we can see that the Se and Te derivatives generate greater amounts of $^1O_2$ when compared to the S derivative (Table 3). This fact may be attributed to a greater favoring of these molecules and possible triplet state population, favoring the ROS formation by the Type II mechanism. As in the formation of singlet oxygen, for the formation of superoxide radicals in DMSO solution, low to moderate values of k_{SO} are also observed. Emphasis is given to **11i** (with the S atom), as it is the derivative that generates the most $O_2^{\bullet-}$ species.

Table 3 Singlet oxygen ($^1O_2$) and superoxide ($O_2^{\bullet -}$) species parameters of compounds **11a–j** in DMSO solution

	Singlet oxygen ($^1O_2$)[a]		Superoxide ($O_2^{\bullet -}$)
Compound	k_{po} (M^{-1} s^{-1}) × 10^{-4}	Φ_Δ (%)	k_{SO} (M^{-1} s^{-1}) × 10^{-5}
11a	1.65	18.0	2.33
11b	1.04	11.0	0.87
11c	3.44	38.0	2.10
11d	3.39	37.0	1.48
11e	0.31	<1.0	2.09
11f	0.43	<1.0	3.16
11g	1.04	11.0	3.12
11h	1.65	18.0	2.04
11i	0.32	<1.0	36.3
11j	1.68	19.0	2.31

[a] Using methylene blue in EtOH as reference (Φ_Δ = 52% and k_{po} = 5.50 × 10^{-2} M^{-1} s^{-1}).[44]

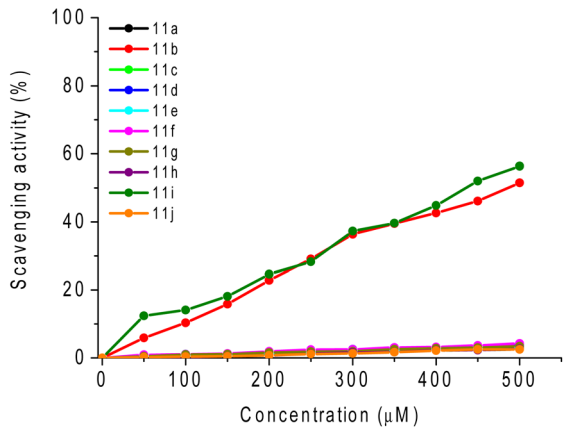

Fig. 7 DPPH scavenging test *versus* concentration (in μM) of compounds **11a–j** and ascorbic acid (AA; reference) in DMSO solution.

Antioxidant properties by DPPH assay

A DPPH scavenging assay was also performed by UV-vis absorption analysis using 2,2-diphenyl-1-picrylhydrazyl (DPPH) as a stable free radical molecule. The percentage of DPPH scavenging of the studied compounds **11a–j** and ascorbic acid (AA; reference molecule), which is an effective scavenger against ROS used as the positive control, are represented in Fig. 7 and Table 4.

Table 4 EC_{50} values in the antioxidant assays (DPPH) for compounds **11a–j**

Compound	EC_{50} (μM)
11a	≥500
11b	486.0
11c	≥500
11d	≥500
11e	≥500
11f	≥500
11g	≥500
11h	≥500
11i	435.0
11j	≥500
Ascorbic acid	10.9

Based on this experiment, derivatives **11b** (R = 4-ClPh) and **11i** (R = SPh) presented the best DPPH activity, but neither is comparable to the standard AA (Table 4). The EC_{50} (half maximal effective concentration) values for these derivatives were calculated, and according to the results obtained in the cyclic voltammetry studies, these derivatives showed the best DPPH activity and had lower oxidation potential values, attributing a better antioxidant activity to these derivatives.

Conclusions

In this paper, we report the synthesis of a series of ten new chalcogen-naphthoquinones-1,2,3-triazoles (**11a–j**) with good to excellent yields, hybridized *via* an efficient three-step methodology involving a series of azides containing chalcogens (**11a–j**) and an alkyne from lawsone (**8**) using the CuAAC reaction. The new compounds were found to be stable in air, easy to handle, and capable of being fully characterized by ^1H and ^{13}C NMR spectroscopy in addition to HRMS. Absorption and steady-state fluorescence emission exhibited UV peaks and emission in the blue region when excited at the least energetic transition of each compound, with varying values of fluorescence quantum yields (Φ_f) and SS values. TDDFT calculations revealed that all compounds had delocalized electron density along the naphthoquinone unit and were not influenced by the attached substituent. In addition, electrochemical analysis, ROS measurement, and DPPH antioxidant properties were analyzed, as these parameters are important for the biological application of this new series of compounds.

Experimental section

For the procedure of isolation and purification of the compounds using column chromatography, the material used was a glass column, silica gel was used as the stationary phase with a 0.063–0.2 mesh by Merck (Darmstadt, Germany) and a suitable solvent or solvent mixture was used as the eluent. The fractions and compounds obtained were analyzed by thin layer chromatography (TLC), using aluminum plates coated with silica gel 60 GF_{254} provided by Merck (Darmstadt, Germany), 0.25 mm thick and with particles between 5 and 40 μm in diameter. The substances separated on the chromatographic plates were visualized using several development methods: in an iodine chamber, in an ultraviolet light chamber, or with a vanillin reagent followed by heating at 110 °C. Melting points were obtained on a Fisatom 430D apparatus and were uncorrected. All solvents and reagents used in the synthesis, purification, and characterization were purchased from commercial sources Sigma-Aldrich, Merck (Darmstadt, Germany), and Synth (Sao Paulo, Brazil) and used without prior purification. APPI-Q-TOFMS measurements were taken on a mass spectrometer equipped with an automatic syringe pump for sample injection. The ^{13}C {^1H} NMR spectra were obtained on Bruker Avance NEO

spectrometer, operating at 500 MHz employing a direct broadband probe at 125 MHz.

Photophysical analysis

Absorption UV-vis analysis of compounds **11a–j** in three solvents (ACN, DCM, and DMSO) were measured using a Shimadzu UV2600 spectrophotometer (slit 1.0 mm). Steady-state fluorescence emission spectra of derivatives **11a–j** in the same solvents were measured with a Horiba Jobin Yvon FluoroMax 4 Plus spectrofluorometer (slit 5.0 mm; Em/Exc), using the high energy (lowest wavelength) transition band as excitation. The fluorescence quantum yield (Φ_F) values of compounds **11a–j** were determined by comparing the corrected fluorescence spectra with the standard 9,10-diphenylanthracene (DPA) in chloroform solution ($\Phi_F = 65\%$, $\lambda_{exc} = 375$ nm) according to the literature.[45]

TDDFT calculations

Electronic and structural properties of compounds **11a–j** were studied through DFT calculations, as implemented in Gaussian 09.[46] Ground state geometrical structures were optimized (energy minimization) through conjugated gradient techniques. The optical absorption spectra were obtained by a single-point TDDFT calculation on the optimized geometries. All calculations were conducted at the wB97XD/6-31G(d,p) level of theory.[47] The polarizable continuum model (PCM) was employed to calculate molecular properties in DMSO.

Electrochemical analysis

Cyclic voltammograms of compounds **11a–j** were recorded with a potentiostat/galvanostat AutoLab Eco Chemie PGSTAT 128 N system at room temperature and under Ar atmosphere in dry dichloromethane (DCM) solution. Electrochemical-grade tetrabutylammonium hexafluorophosphate ($TBAPF_6$; 0.1 M) was used as a supporting electrolyte, using a glassy carbon working electrode; a platinum wire auxiliary electrode and a platinum wire pseudo-reference electrode. To monitor the reference electrode, the ferrocenium/ferrocene redox couple was used as an internal reference.[48]

ROS generation

The singlet oxygen quantum yield (Φ_Δ) of compounds **11a–j** was recorded by a DPBF photooxidation assay in DMSO solution. In order to measure singlet oxygen generation, UV-vis spectra of each solution were recorded at different exposure times (0 to 900 s, white-light LED source by irradiance of 50 mW cm^{-2} and a total light dosage of 45 J cm^{-2}). The Φ_Δ values were calculated according to the literature, using methylene blue in ethanol as the standard ($\Phi_{\Delta std} = 52\%$).[44,49]

The superoxide radical ($O_2^{\bullet-}$) formation in DMSO solutions was evaluated by an NBT (Nitro Blue Tetrazolium Chloride) reduction experiment to detect the formation of superoxide radical species. This experiment was carried out using the same conditions in the literature.[50] Compounds **11a–j** were irradiated under aerobic conditions with a white-light LED source for a total period of 30 min (irradiance of 50 mW cm^{-2} and a total light dosage of 90 J cm^{-2}). The superoxide formation was monitored by following the increase of the absorbance close to 560 nm. The superoxide generation constant (k_{SO}) can be obtained from the slope in the plot of $Abs_{formazan}$ *versus* time (Fig. S79†).

DPPH antioxidant assay

The free radical scavenging ability of derivatives **11a–j** was determined using the DPPH assay method according to the literature.[51] The DPPH assay method are presented in the ESI section.†

Synthetic procedures

General procedure for the synthesis of propargylated lawsone.[34] In a round bottom flask, 5.75 mmol (1.0 g) of lawsone **8**, 1.2 eq. (0.95 g) K_2CO_3, and 50 mL of DMF were combined. The mixture was stirred for 15 minutes, then 10 eq. propargyl bromide (7.0 mL) was added, then the solution was heated at 60 °C for 12 hours. Subsequently, after cooling to room temperature, ethyl acetate was added to the mixture, and this phase was washed with brine (3 × 100 mL); the organic phase was dried with anhydrous sodium sulfate then filtered, and the solvent was evaporated under reduced pressure. The product was purified by column chromatography on silica gel, using a gradient hexane/ethyl acetate (9 : 1) mixture as the eluent.

*2-(Prop-2-yn-1-yloxy)naphthalene-1,4-dione (compound **9**).* 0.72 g, yield 60%, yellow solid, m.p. 150–151 °C. ^{1}H NMR ($CDCl_3$, 500 MHz) δ (ppm) = 8.15–8.08 (m, 2H), 7.77–7.71 (m, 2H), 6.36 (s, 1H), 4.80 (d, $J = 2.5$ Hz; 2H), 2.65 (t, $J = 2.5$ Hz; 1H). ^{13}C NMR ($CDCl_3$, 125 MHz) δ = 184.68, 179.79, 158.05, 134.36, 133.45, 131.88, 131.05, 126.73, 126.22, 111.65, 78.18, 75.43, 56.73.

General procedure for the synthesis of azides.[35] At room temperature, sodium azide (1.5 mmol; 0.097 g) was added to a solution of chloromethyl arylchalcogenides **13a–j** (1 mmol) in CH_3CN (1.5 mL) and 18-crown-6 (0.20 mmol; 0.053 g). The mixture was then stirred for 48 hours at this temperature in a nitrogen atmosphere. The solution was then diluted with H_2O (10 mL) and washed with CH_2Cl_2 (3 × 10 mL). The organic layers were combined, dried over $MgSO_4$, and vacuum concentrated. Flash chromatography on silica gel with hexanes as the eluent was used to purify the residue. The spectral data of the prepared products are listed below.

Characterization

*(Azidomethyl)(phenyl)selane (compound **10a**).* 0.1007 g, yield: 95%, yellow oil, ^{1}H NMR ($CDCl_3$, 500 MHz) δ = 7.64–7.60 (m, 2H), 7.33–7.29 (m, 3H), 4.60 (s, 2H). ^{13}C NMR ($CDCl_3$, 125 MHz) δ = 133.93, 129.34, 128.13, 48.70.

*(Azidomethyl)(4-chlorophenyl)selane (compound **10b**).* 0.1104 g, yield: 89%, yellow oil, ^{1}H NMR ($CDCl_3$, 500 MHz) δ = 7.55–7.53 (m, 2H), 7.32–7.27 (m, 2H), 4.59 (s, 2H). ^{13}C NMR ($CDCl_3$, 125 MHz) δ = 135.33, 135.02, 134.56, 129.51, 126.47, 48.90.

*(Azidomethyl)(p-tolyl)selane (compound **10c**).* 0.1017 g, yield: 95%, yellow oil, ^{1}H NMR ($CDCl_3$, 500 MHz) δ = 7.55 (d, 2H), 7.14 (d, 2H), 4.58 (s, 2H), 2.37 (s, 3H). ^{13}C NMR ($CDCl_3$, 125 MHz) δ = 138.42, 134.48, 130.18, 124.60, 48.98, 21.19.

*(Azidomethyl)(4-methoxyphenyl)selane (compound **10d**).* 0.1375 g, yield: 88%, orange oil, ^{1}H NMR ($CDCl_3$, 500 MHz) δ = 7.58–7.55 (m, 2H), 6.87–6.83 (m, 2H), 4.48 (s, 2H), 3.78 (s, 3H). ^{13}C NMR ($CDCl_3$, 125 MHz) δ = 160.19, 136.83, 134.60, 118, 24, 115.05, 55.33, 49.45. HRMS (APPI+) *m*/*z*: calculated for $C_8H_9N_3OSe$ $[M + Na]^+$: 265.98; found: 265.26.

*(Azidomethyl)(mesityl)selane (compound **10e**).* 0.1168 g, yield: 92%, yellow oil, ^{1}H NMR ($CDCl_3$, 500 MHz) δ = 6.94 (d, 2H), 4.68 (s, 1H), 4.37 (s, 1H), 2.54 (d, 6H), 2.26 (d, 3H). ^{13}C NMR ($CDCl_3$, 125 MHz) δ = 143.27, 139.23, 128.78, 126.21, 48.50, 24.57, 20.99. HRMS (APPI+) *m*/*z*: calculated for $C_{10}H_{13}N_3Se$ $[M + Na]^+$: 277.20; found: 277.23.

*(Azidomethyl)(butyl)selane (compound **10f**).* 0.0835 g, yield: 87%, yellow oil, ^{1}H NMR ($CDCl_3$, 500 MHz) δ = 2.56 (t, 2H), 1.64 (q, 2H), 1.42 (sext, 2H), 1.26 (s, 2H), 0.92 (qt, 3H). ^{13}C NMR ($CDCl_3$, 125 MHz) δ = 32.79, 29.69, 23.63, 23.07, 13.60. HRMS (APPI+) *m*/*z*: calculated for $C_5H_{11}N_3Se$ $[M + K]^+$: 231.23; found: 231.15.

*2-((Azidomethyl)selanyl)thiophene (compound **10g**).* 0.0981 g, yield: 90%, brown oil, ^{1}H NMR ($CDCl_3$, 500 MHz) δ = 7.46 (d, 1H), 7.33 (d, 1H), 7.02 (dd, 1H), 4.73 (s, 2H). ^{13}C NMR ($CDCl_3$, 125 MHz) δ = 132.21, 127.45, 123.46, 116.63, 46.44. HRMS (APPI+) *m*/*z*: calculated for $C_5H_5N_3SSe$ $[M + H]^+$: 219.15; found: 219.03.

*(Azidomethyl)(naphthalen-2-yl)selane (compound **10h**).* 0.1139 g, yield: 87%, brown oil, ^{1}H NMR ($CDCl_3$, 500 MHz) δ = 8.41 (d, 1H), 8.36–8.33 (m, 1H), 7.95 (d, 1H), 7.88–7.83 (m, 3H), 7.78 (d, 1H), 4.60 (s, 2H). ^{13}C NMR ($CDCl_3$, 125 MHz) δ = 134.60, 132.21, 129.76, 128.81, 128.65, 128.44, 127.13, 127.08, 126.85, 126.36, 126.12, 48.61. HRMS (APPI+) *m*/*z*: calculated for $C_{11}H_9N_3Se$ $[M + K]^+$: 301.28; found: 301.30.

*(Azidomethyl)(phenyl)sulfane (compound **10i**).* 0.0763 g, yield: 93%, yellow oil, ^{1}H NMR ($CDCl_3$, 500 MHz) δ = 7.49–7.46 (m, 2H), 7.34–7.30 (m, 2H), 7.29–7.26 (m, 1H), 4.49 (s, 2H). ^{13}C NMR ($CDCl_3$, 125 MHz) δ = 136.97, 132.21, 128.22, 121.59, 51.20. HRMS (APPI+) *m*/*z*: calculated for $C_7H_7N_3S$ $[M + K]^+$: 206.9998; found: 206.9464.

*(Azidomethyl)(phenyl)tellane (compound **10j**).* 0.0871 g, yield: 67%, orange oil, ^{1}H NMR ($CDCl_3$, 500 MHz) δ = 7.87–7.85 (m, 2H), 7.39–7.35 (m, 1H), 7.30–7.26 (m, 2H), 4.89 (s, 2H). ^{13}C NMR ($CDCl_3$, 125 MHz) δ = 138.92, 129.48, 128.70, 112.51, 60.37. HRMS (APPI+) *m*/*z*: calculated for $C_7H_7N_3Te$ $[M + K]^+$: 301.94; found: 301.37.

General procedure for the synthesis of chalcogen-naphthoquinones-1,2,3-triazoles.[38] In a round bottom flask, the azide (1.5 eq.) was added to the solvent mixture H_2O : CH_2Cl_2 (2.0 mL). The alkyne (0.25 mmol; 0.053 g), $CuSO_4 \cdot 5H_2O$ (1% mol), and sodium ascorbate (10% mol) were then added in that order. The mixture was stirred at room temperature until all reagents were consumed, then the product was extracted with dichloromethane after 24 hours (2 × 20 mL). The organic phase was finally dried with anhydrous sodium sulfate and filtered, and the solvent was evaporated under reduced pressure. The product was purified using column chromatography and an eluent gradient of hexane and ethyl acetate.

Characterization

*2-((1-((Phenylselanyl)methyl)-1H-1,2,3-triazol-4-yl)methoxy) naphthalene-1,4-dione (compound **11a**).* 0.0742 g, yield: 70%, orange solid, m.p. 117–118 °C. ^{1}H NMR ($CDCl_3$, 500 MHz) δ = 8.11–8.06 (m, 2H), 7.76–7.69 (m, 2H), 7.64 (s, 1H), 7.47–7.45 (m, 2H), 7.33–7.27 (m, 3H), 6.37 (s, 1H), 5.71–5.69 (m, 2H), 5.21 (s, 2H). ^{13}C NMR ($CDCl_3$, 125 MHz) δ = 184.63, 179.83, 158.77, 141.94, 134.73, 134.35, 133.38, 132.25, 131.90, 131.02, 129.66, 129.08, 127.08, 126.63, 126.19, 123.46, 111.20, 62.80, 44.74. HRMS (APPI+) *m*/*z*: calculated for $C_{20}H_{15}N_3O_3Se$ $[M + Na]^+$: 448.0198; found: 448.0160.

*2-((1-(((4-Chlorophenyl)selanyl)methyl)-1H-1,2,3-triazol-4-yl) methoxy)naphthalene-1,4-dione (compound **11b**).* 0.0725 g, yield: 63%, orange solid, m.p. 185–186 °C. ^{1}H NMR ($CDCl_3$, 500 MHz) δ = 8.11–8.06 (m, 2H), 7.75–7.68 (m, 3H), 7.40–7.36 (m, 2H), 7.26–7.24 (m, 2H), 6.35 (s, 1H), 5.66 (s, 2H), 5.21 (s, 2H). ^{13}C NMR ($CDCl_3$, 125 MHz) δ = 184.65, 179.83, 158.78, 142.26, 136.21, 135.79, 134.38, 133.42, 131.93, 131.05, 129.92, 128.79, 126.70, 126.23, 124.98, 111.22, 62.84, 44.81. HRMS (APPI+) *m*/*z*: calculated for $C_{20}H_{14}ClN_3O_3Se$ $[M]^+$: 459.9978; found: 459.9973.

*2-((1-((p-Tolylselanyl)methyl)-1H-1,2,3-triazol-4-yl)methoxy) naphthalene-1,4-dione (compound **11c**).* 0.0654 g, yield: 60%, yellow solid, m.p. 156–157 °C. ^{1}H NMR ($CDCl_3$, 500 MHz) δ = 8.09–8.04 (m, 2H), 7.74–7.67 (m, 2H), 7.58 (s, 1H), 7.30 (d, J = 8.2 Hz; 2H), 7.05 (d, J = 8.2 Hz; 2H), 6.35 (s, 1H), 5.62 (s, 2H), 5.19 (s, 2H), 2.28 (s, 3H). ^{13}C NMR ($CDCl_3$, 125 MHz) δ = 184.64, 179.85, 158.78, 141.90, 139.46, 135.07, 134.36, 133.38, 131.92, 131.04, 130.48, 126.64, 126.21, 123.36, 111.23, 62.85, 45.01, 21.17. HRMS (APPI+) *m*/*z*: calculated for $C_{21}H_{17}N_3O_3Se$ $[M + Na]^+$: 462.0298; found: 462.0318.

*2-((1-(((4-Methoxyphenyl)selanyl)methyl)-1H-1,2,3-triazol-4-yl) methoxy)naphthalene-1,4-dione (compound **11d**).* 0.0689 g, yield: 61%, yellow solid, m.p. 137–138 °C. ^{1}H NMR ($CDCl_3$, 500 MHz) δ = 8.11–8.07 (m, 2H), 7.77–7.69 (m, 2H), 7.61 (s, 1H), 7.36–7.34 (m, 2H), 6.82–6.79 (m, 2H), 6.38 (s, 1H), 5.60 (s, 2H), 5.22 (s, 2H), 3.78 (s, 3H). ^{13}C NMR ($CDCl_3$, 125 MHz) δ = 184.65, 179.85, 160.66, 158.81, 141.85, 137.24, 134.35, 133.38, 131.91, 131.03, 126.63, 126.20, 123.41, 117.03, 115.30, 111.20, 62.86, 55.28, 45.31. HRMS (APPI+) *m*/*z*: calculated for $C_{21}H_{17}N_3O_4Se$ $[M + Na]^+$: 478.0298; found: 478.0264.

*2-((1-((Mesitylselanyl)methyl)-1H-1,2,3-triazol-4-yl)methoxy) naphthalene-1,4-dione (compound **11e**).* 0.0742 g, yield: 64%, light yellow solid, m.p. 127–128 °C. ^{1}H NMR ($CDCl_3$, 500 MHz) δ = 8.14–8.09 (m, 2H), 7.78–7.71 (m, 2H), 7.29 (s, 1H), 6.87 (s, 2H), 6.37 (s, 1H), 5.48 (s, 2H), 5.21 (s, 2H), 2.27 (s, 6H), 2.21 (s, 3H). ^{13}C NMR ($CDCl_3$, 125 MHz) δ = 184.61, 179.83, 158.69, 143.31, 141.81, 139.94, 134.37, 133.39, 131.93, 131.05, 129.01, 126.63, 126.24, 125.15, 123.30, 111.23, 62.75, 43.40, 24.07, 20.93. HRMS (APPI+) *m*/*z*: calculated for $C_{23}H_{21}N_3O_3Se$ $[M + Na]^+$: 490.0598; found: 490.0642.

*2-((1-((Butylselanyl)methyl)-1H-1,2,3-triazol-4-yl)methoxy) naphthalene-1,4-dione (compound **11f**).* 0.0534 g, yield: 53%, dark brown solid, m.p. 101–102 °C. ^{1}H NMR ($CDCl_3$, 500 MHz) δ = 8.12–8.07 (m, 2H), 7.97 (s, 1H), 7.77–7.69 (m, 2H), 6.42 (s, 1H), 5.50 (s, 2H), 5.26 (s, 2H), 2.70 (t, J = 7.4 Hz; 2H), 1.62 (qui, J = 7.4

Hz; 2H), 1.36 (sxt, J = 7.4 Hz; 2H), 0.88 (t, J = 7.4 Hz; 3H) ^{13}C NMR ($CDCl_3$, 125 MHz) δ = 184.67, 179.85, 158.86, 142.21, 134.33, 133.37, 131.90, 131.03, 126.64, 126.18, 123.45, 111.20, 62.89, 40.07, 31.88, 25.38, 22.75, 13.45. HRMS (APPI+) *m*/*z*: calculated for $C_{18}H_{19}N_3O_3Se$ $[M + Na]^+$: 428.0498; found: 428.0478.

*2-((1-((Thiophen-2-ylselanyl)methyl)-1H-1,2,3-triazol-4-yl) methoxy)naphthalene-1,4-dione (compound **11g**).* 0.0773 g, yield: 68%, dark brown solid, m.p. 67–68 °C. ^{1}H NMR ($CDCl_3$, 500 MHz) δ = 8.13–8.08 (m, 2H), 7.77–7.70 (m, 2H), 7.59 (s, 1H), 7.45–7.44 (m, 1H), 7.10–7.09 (m, 1H), 6.99–6.97 (m, 1H), 6.39 (s, 1H), 5.57 (s, 2H), 5.25 (s, 2H). ^{13}C NMR ($CDCl_3$, 125 MHz) δ = 184.64, 179.87, 158.76, 141.99, 138.00, 134.37, 133.40, 133.19, 131.92, 131.04, 128.66, 126.65, 126.22, 123.41, 120.23, 111.29, 62.82, 46.76. HRMS (APPI+) *m*/*z*: calculated for $C_{18}H_{13}N_3O_3SSe$ $[M + Na]^+$: 453.9698; found: 453.9737.

*2-((1-((Naphthalen-2-ylselanyl)methyl)-1H-1,2,3-triazol-4-yl) methoxy)naphthalene-1,4-dione (compound **11h**).* 0.0826 g, yield: 70%, brown solid, m.p. 135–136 °C. ^{1}H NMR ($CDCl_3$, 500 MHz) δ = 8.25–8.23 (m, 1H), 8.11–8.07 (m, 2H), 7.87–7.85 (m, 1H), 7.82–7.80 (m, 1H), 7.77–7.69 (m, 3H), 7.55–7.46 (m, 2H), 7.36–7.33 (m, 1H), 6.31 (s, 1H), 5.68 (s, 2H), 5.30 (s, 2H). ^{13}C NMR ($CDCl_3$, 125 MHz) δ = 184.63, 179.79, 158.72, 141.66, 135.92, 134.34, 134.10, 133.37, 131.92, 131.04, 130.79, 128.91, 127.48, 127.24, 126.63, 126.20, 125.89, 123.53, 111.12, 62.64, 44.27. HRMS (APPI+) *m*/*z*: calculated for $C_{24}H_{17}N_3O_3Se$ $[M + Na]^+$: 498.0298; found: 498.0323.

*2-((1-((Phenylthio)methyl)-1H-1,2,3-triazol-4-yl)methoxy) naphthalene-1,4-dione (compound **11i**).* 0.0761 g, yield: 81%, red oil, ^{1}H NMR ($CDCl_3$, 500 MHz) δ = 8.11–8.05 (m, 2H), 7.76–7.69 (m, 3H), 7.33–7.31 (m, 2H), 7.29–7.27 (m, 2H), 6.36 (s, 1H), 5.64 (s, 2H), 5.22 (s, 2H). ^{13}C NMR ($CDCl_3$, 125 MHz) δ = 184.64, 179.85, 158.77, 142.07, 134.36, 133.39, 132.28, 131.93, 131.52, 131.04, 129.59, 128.87, 126.66, 126.21, 123.07, 111.23, 62.84, 54.08. HRMS (APPI+) *m*/*z*: calculated for $C_{20}H_{15}N_3O_3S$ $[M + Na]^+$: 400.0698; found: 400.0726.

*2-((1-((Phenyltellanyl)methyl)-1H-1,2,3-triazol-4-yl)methoxy) naphthalene-1,4-dione (compound **11j**).* 0.0354 g, yield: 30%, orange oil, ^{1}H NMR ($CDCl_3$, 500 MHz) δ = 8.13–8.08 (m, 2H), 7.77–7.72 (m, 5H), 7.57 (s, 1H), 7.37–7.35 (m, 1H), 7.29–7.28 (m, 1H), 6.39 (s, 1H), 5.88 (s, 2H), 5.20 (s, 2H). ^{13}C NMR ($CDCl_3$, 125 MHz) δ = 180.04, 167.97, 158.29, 138.21, 136.07, 134.59, 133.69, 132.68, 132.13, 131.30, 131.09, 130.17, 129.72, 129.02, 126.97, 126.46, 111.89, 68.39, 56.95. HRMS (APPI+) *m*/*z*: calculated for $C_{20}H_{15}N_3O_3Te$ $[M + H]^+$: 475.02; found: 475.15.

Conflicts of interest

There are no conflicts to declare.

Acknowledgements

This project was supported by the funding agencies: CAPES (88887.505029/2020-00 and Finance Code 001), CNPq (306011/2020-4, 301873/2019-4, 310656/2021-4, 403210/2021-6 and 305458/2021-3), FAPERJ (E-26/202.911/2019, E-26/010.002250/2019, E-26/210.325/2022, E-26/200.235/2023), FAPERGS (21/2551-0002114-4) and INCT-Catálise.

References

1 C. Viegas-Junior, E. J. Barreiro and C. A. M. Fraga, *Curr. Med. Chem.*, 2007, **14**, 1829–1852.

2 C. G. Wermuth, *The practice of medicinal chemistry*, Academic Press, London, 2nd edn, 2008.

3 (*a*) R. H. Thomson, *Naturally Occurring Quinones*. Academic Press, New York, 1971; (*b*) R. H. Thompson, *Naturally Occuring Quinones IV: Recents Advances*, Champman & Hall, London, 1997; (*c*) E. J. Barreiro, J. E. M. da Silva and C. A. M. Fraga, *Quim. Nova*, 1996, **19**, 641–650.

4 (*a*) J. L. Bolton and T. Dunlap, *Chem. Res. Toxicol.*, 2017, **30**, 13–37; (*b*) P. S. Cordeiro, I. C. Chipoline, R. C. Ribeiro, D. R. Pinho, V. F. Ferreira, F. C. D. Silva and V. Nascimento, *J. Braz. Chem. Soc.*, 2022, **33**, 111–127; (*c*) I. Mancini, J. Vigna, D. Sighel and A. Defant, *Molecules*, 2022, **27**, 4948–4990; (*d*) V. Sebastián-Pérez, P. M. Iturrate, M. Nácher-Vázquez, L. Nóvoa, C. Pérez, N. E. Campillo, C. Gil and L. Rivas, *Biomedicines*, 2022, **10**, 1136–1163; (*e*) L. P. Borba-Santos, C. D. Nicoletti, T. Vila, P. G. Ferreira, C. F. Araújo-Lima, B. V. D. Galvão, I. Felzenszwalb, W. Souza, F. C. Silva, V. F. Ferreira, D. O. Futuro and S. Rozental, *Braz. J. Microbiol.*, 2022, **53**, 749–758.

5 M. N. Silva, V. F. Ferreira and M. C. B. V. Souza, *Quim. Nova*, 2003, **26**, 407–416.

6 (*a*) J. K. F. Andrade, A. J. S. Góes, V. X. Barbosa, M. S. L. Silva, M. A. M. Donato, C. A. Peixoto, G. C. G. Militão and T. G. Silva, *Chem.-Biol. Interact.*, 2022, **365**, 110057; (*b*) J. M. M. Del Corral, M. A. Castro, M. Gordaliza, M. L. Marton, S. A. Gualberto, A. M. Gamito, C. Vuevas and A. San Feliciano, *Bioorg. Med. Chem.*, 2005, **13**, 631; (*c*) I. A. C. Araújo, R. C. Paula, C. L. Alves, K. F. Faria, M. M. Oliveira, G. G. Mendes, E. M. F. A. Dias, R. R. Riberio, A. B. Oliveira and S. M. Silva, *Exp. Parasitol.*, 2019, **199**, 67–73; (*d*) V. V. Vale, J. N. Cruz, G. M. R. Viana, M. M. Póvoa, D. S. B. Brasil and M. F. Dolabela, *Med. Chem. Res.*, 2020, **29**, 487–494; (*e*) C. Espinosa-Bustos, M. O. Pérez, A. Gonzalez-Gonzalez, A. M. Zarate, G. Rivera, J. A. Belmont-Diaz, E. Saavedra, M. A. Cuellar, K. Vázquez and C. O. Salas, *Pharmaceutics*, 2022, **14**, 1121; (*f*) K. W. Stagliano, A. Emadi, Z. Lu, H. C. Malinakova, B. Twenter, M. Yu, I. E. Holland, A. M. Rom, J. S. Harwood, R. Amin, A. Johnson and P. Yves, *Bioorg. Med. Chem.*, 2006, **14**, 5651–5665.

7 Y. G. Paiva, R. Ferreira, T. L. Silva, E. Labbe, O. Buriez, C. Amatore and M. O. F. Goulart, *Curr. Top. Med. Chem.*, 2015, **15**, 136–162.

8 P. Dahiya, D. K. Nayak, T. Mukherjee and H. Pal, *J. Photochem. Photobiol., A*, 2007, **186**, 218–228.

9 (*a*) P. Mohanty, P. P. Dash, R. Behura, S. Behera, A. K. Barick and B. R. Jali, *Lett. Appl. NanoBioScience*, 2023, **12**, 123–142; (*b*) V. L. A. Santos, A. A. Gonsalves, D. G. Guimarães, S. S. Simplicio, H. P. Oliveira, L. P. S. Ramos, M. P. Costa, F. C. E. Oliveira, C. Pessoa and C. R. M. Araújo, *Molecules*,

3008, **8**, 2023; (*c*) G. G. Dias, A. King, F. Moliner, M. Vendrell and E. N. Da Silva Júnior, *Chem. Soc. Rev.*, 2018, **47**, 12–27.

10 (*a*) J. Wang, D. Qin, J. Lan, Y. Cheng, S. Zhang, Q. Guo, J. Wu, D. Wu and J. You, *Chem. Commun.*, 2015, **51**, 6337–6339; (*b*) V. Dixit, A. Sharma, A. Jangid and N. Jain, *Adv. Synth. Catal.*, 2023, **365**, 892–899; (*c*) K. K. Chenab, B. Sohrabi, M. R. Z. Meymian and S. V. Mousavi, *Mater. Res. Express*, 2019, **6**, 085537; (*d*) S. A. Mahadik, H. M. Pathan, S. Salunke-Gawali and R. J. Butcher, *J. Alloys Compd.*, 2020, **845**, 156279.

11 B. M. Rodrigues, C. C. Diniz, V. N. Da Rocha, M. H. Köhler, G. P. Brandão, L. A. Machado, E. N. Da Silva Júnior and B. A. Iglesias, *RSC Adv.*, 2023, **13**, 11121.

12 (*a*) K. S. S. Campanholi, A. P. Gerola, B. H. Vilsinski, E. L. Oliveira, F. A. P. Morais, B. R. Rabello, G. Braga, I. R. Calori, E. L. Silva, N. Hioka and W. Caetano, *Dyes Pigm.*, 2018, **157**, 238–250; (*b*) L. A. Machado, E. R. S. Paz, M. H. Araujo, L. D. Almeida, I. A. O. Bozzi, G. G. Dias, C. L. M. Pereira, L. F. Pedrosa, F. Fantuzzi, F. T. Martins, L. A. Cury and E. N. S. Júnior, *Eur. J. Org Chem.*, 2022, **2022**, e202200590; (*c*) C. M. Souza, R. C. Silva, P. O. Fernandes, J. D. S. Filho, H. A. Duarte, M. H. Araujo, C. A. Simone, S. L. Castro, R. F. S. Menna-Barreto, C. P. Demicheli and E. N. S. Júnior, *New J. Chem.*, 2017, **41**, 3723–3731; (*d*) T. B. Gontijo, R. P. Freitas, G. F. Lima, L. C. D. Rezende, L. F. Pedrosa, T. L. Silva, M. O. F. Goulart, B. C. Cavalcanti, C. Pessoa, M. P. Bruno, J. R. Corrêa, F. S. Emery and E. N. S. Júnior, *Chem. Commun.*, 2016, **52**, 13281–13284.

13 G. G. Dias, P. V. B. Pinho, H. A. Duarte, J. M. Resende, A. B. B. Rosa, J. R. Correa, B. A. D. Neto and E. N. S. Júnior, *RSC Adv.*, 2016, **6**, 76056–76063.

14 N. Trometer, B. Cichoki, Q. Chevalier, J. Pécourneau, J. Strub, A. Hemmerlin, A. Specht, E. Davioud-Charvet and M. Elhabiri, *J. Org. Chem.*, 2023, DOI: **10.1021/acs.joc.3c00620**.

15 (*a*) J. Comasseto, Vinylic selenides, *J. Org. Chem.*, 1983, **253**, 131–181; (*b*) T. Kanda, L. Engman, I. A. Cotgreave and G. Powis, *J. Org. Chem.*, 1999, **64**, 8161–8169; (*c*) M. Parnham and E. Graf, *Prog. Drug Res.*, 1991, **36**, 10–47; (*d*) C. Nogueira, G. Zeni and J. Rocha, *Chem. Rev.*, 2004, **104**, 6255–6285; (*e*) A. A. Vieira, I. R. Brandão, W. O. Valença, C. A. Simone, B. C. Cavalcanti, C. Pessoa, T. R. Carneiro, A. L. Braga and E. N. Da Silva, *Eur. J. Med. Chem.*, 2015, **101**, 254–265.

16 (*a*) Y. N. Lee, P. Attri, S. S. Kim, S. J. Lee, J. H. Kim, T. J. Cho and I. T. Kim, *New J. Chem.*, 2017, **41**, 6315; (*b*) B. Fan, F. Lin, X. Wu, Z. Zhu and A. K. Y. Jen, *Acc. Chem. Res.*, 2021, **54**, 3906.

17 D. B. Paixão, E. G. O. Soares, H. D. Salles, C. D. G. Silva, D. S. Rampon and P. H. Schneider, *Org. Chem. Front.*, 2022, **9**, 5225.

18 C. H. Silveira, M. G. Fronza, R. A. Balaguez, A. M. E. Larroza, L. Savegnago, D. F. Back, B. A. Iglesias and D. Alves, *Dyes Pigm.*, 2021, **185**, 108910.

19 I. A. Graciano, A. S. Carvalho, F. C. Silva and V. F. Ferreira, *Med. Chem.*, 2022, **18**, 521–535.

20 R. Begam, A. Shajahan, B. Shefin and V. Murugan, *J. Mol. Struct.*, 2022, **1254**, 132364.

21 L. Dehestani, N. Ahangar, S. M. Hashemi, H. Irannejad, P. H. Masihi, A. Shakiba and S. Emami, *Bioorg. Chem.*, 2018, **78**, 119–129.

22 Y. Nural, S. Ozdemir, M. S. Yalcin, B. Demir, H. Atabey, Z. Seferoglu and A. Ece, *Bioorg. Med. Chem. Lett.*, 2022, **55**, 128453.

23 P. Yadav, C. P. Kaushik and A. Kumar, *Synth. Commun.*, 2022, **52**, 2149–2162.

24 S. Jurado, O. Illa, A. Álvarez-Larena, C. Pannecouque, F. Busqué and R. Alibés, *J. Org. Chem.*, 2022, **87**, 15166–15177.

25 M. Chahal, C. P. Kaushik, R. Luxmi, D. Kumar and A. Kumar, *Med. Chem. Res.*, 2023, **32**, 85–98.

26 R. B. Peres, M. M. Batista, A. L. R. Bérenguer, F. C. Camillo, M. R. Figueiredo and M. N. C. Soeiro, *Pharmaceutics*, 2023, **15**, 1535.

27 S. K. Kancharla, S. Birudaraju, A. Pal, L. K. Reddy, E. R. Reddy, S. K. Vagolu, D. Sriram, K. B. Bonige and R. B. Korupolub, *New J. Chem.*, 2022, **46**, 2863–2874.

28 E. M. Othman, E. A. Fayed, E. M. Husseiny and H. S. Abulkhair, *New J. Chem.*, 2022, **46**, 12206–12216.

29 S. Jana, S. Iram, J. Thomas, M. Q. Hayat, C. Pannecouque and W. Dehaen, *Molecules*, 2017, **22**, 303–315.

30 P. Silalai, S. Jaipea, J. Tocharus, A. Athipornchai, A. Suksamrarn and R. Saeeng, *ACS Omega*, 2022, **7**, 24302–24316.

31 (*a*) M. C. Joseph, I. A. Kotze, N. J. Nnaji, A. J. Swarts and S. F. Mapolie, *Organometallics*, 2022, **41**, 3546–3556; (*b*) L. Sacarescu, M. Dascalu, A.-L. Chibac-Scutaru and G. Roman, *J. Photochem. Photobiol., A*, 2022, **433**, 114160; (*c*) M. Rabha, S. K. Sheet, B. Sen, I. Konthoujam, K. Aguan and S. Khatua, *ChemistrySelect*, 2023, **8**, e202204643.

32 N. E. Safronov, B. D. Tsyrenova, A. S. Minin, E. Benassi, V. G. Nenajdenko and N. P. Belskaya, *Dyes Pigm.*, 2023, **217**, 111405.

33 (*a*) G. A. M. Jardim, I. A. O. Bozzi, W. X. C. Oliveira, C. Mesquita-Rodrigues, R. F. S. Menna-Barreto, R. A. Kumar, E. Gravel, R. Doris, A. L. Braga and R. N. Da Sila Júnior, *New J. Chem.*, 2019, **43**, 13751–13763; (*b*) G. A. M. Jardim, D. J. B. Lima, W. O. Valença, B. C. Cavalcanti, C. Pessoa, J. Rafique, A. L. Braga, C. Jacob, E. N. Da Silva Júnior and E. H. G. Cruz, *Molecules*, 2017, **30**, 83.

34 D. R. Rocha, K. Mota, I. M. C. B. Silva, V. F. Ferreira, S. B. Ferreira and F. C. Silva, *Tetrahedron*, 2014, **70**, 3266–3270.

35 X. Huang and D. Duan, *Synlett*, 1998, **11**, 1191–1930.

36 N. Seus, M. T. Saraiva, E. E. Alberto, L. Savegnano and D. Alves, *Tetrahedron*, 2012, **68**, 10419–10425.

37 (*a*) V. V. Rostovtsev, L. G. Green, V. V. Fokin and K. B. Sharpless, *Angew. Chem., Int. Ed.*, 2002, **41**, 2596; (*b*) C. W. TornØe, C. Christensen and M. Meldal, *J. Org. Chem.*, 2002, **67**, 3057; (*c*) J. H. van Maarseveen, V. D. Bock and H. Hiemstra, *Eur. J. Org Chem.*, 2006, **2006**, 51.

38 K. B. Sharpless, H. C. Kolb and M. G. Finn, *Angew. Chem., Int. Ed.*, 2001, **40**, 2004.

39 (*a*) S. Parveen, F. Naaz, D. L. V. K. Prasad and G. Anantharaman, *Analyst*, 2023, **148**, 2362–2374; (*b*) R. B. Silva, F. L. Coelho, H. C. S. Júnior, J. C. Germino, T. D. Z. Atvars, F. S. Rodembusch, L. G. T. A. Duarte and P. H. Schneider, *J. Fluoresc.*, 2023, DOI: 10.1007/s10895-023-03358-1; (*c*) A. Abdillah, P. M. Sonawane, D. Kim, D. Mametov, S. Shimodaira, Y. Park and D. G. Churchill, *Molecules*, 2021, **26**, 692; (*d*) X. Chen, T. Pradhan, F. Wang, J. S. Kim and J. Yoon, *Chem. Rev.*, 2012, **112**, 1910–1956; (*e*) J. Fernández-Lodeiro, M. F. Pinatto-Botelho, A. A. Soares-Paulino, A. C. Gonçalves, B. A. Sousa, C. Princival and A. A. Dos Santos, *Dyes Pigm.*, 2014, **110**, 28–48; (*f*) G. C. Hoover and D. S. Seferos, *Chem. Sci.*, 2019, **10**, 9182.

40 (*a*) A. C. Bevilacqua, M. H. Köhler and P. C. Piquini, *J. Phys. Chem. C*, 2019, **123**, 20869–20876; (*b*) A. C. Bevilacqua, M. H. Köhler, B. A. Iglesias and P. C. Piquini, *Comput. Mater. Sci.*, 2019, **158**, 228–234; (*c*) V. N. Rocha, M. H. Köhler, K. Nagata and P. C. Piquini, *Spectrochim. Acta, Part A*, 2023, **293**, 122500.

41 J. G. Leal, A. C. Sauer, J. C. P. Mayer, S. T. Stefanello, D. F. Gonçalves, F. A. A. Soares, B. A. Iglesias, D. F. Back, O. E. D. Rodrigues and L. Dornelles, *New J. Chem.*, 2017, **41**, 5875–5883.

42 J. S. S. Neto, B. A. Iglesias, D. F. Back and G. Zeni, *Adv. Synth. Catal.*, 2016, **358**, 3572–3585.

43 I. C. Chipoline, B. F. A. B. Brasil, J. S. S. Neto, M. Valli, R. Krogh, A. R. Cenci, K. F. Teixeira, E. Zapp, D. Brondani, L. L. G. Ferreira, A. D. Andricopulo, A. S. Oliveira and V. Nascimento, *Eur. J. Med. Chem.*, 2022, **243**, 114687.

44 R. W. Redmond and J. N. Gamlin, *Photochem. Photobiol.*, 1999, **70**, 391–475.

45 G. Heinrich, S. Schoof and H. Gusten, *J. Photochem.*, 1974, **3**, 315–320.

46 M. J. Frisch, G. W. Trucks, H. B. Schlegel, G. E. Scuseria, M. A. Robb, J. R. Cheeseman, G. Scalmani, V. Barone, B. Mennucci, G. A. Petersson, H. Nakatsuji, M. Caricato, X. Li, H. P. Hratchian, A. F. Izmaylov, J. Bloino, G. Zheng, J. L. Sonnenberg, M. Hada, M. Ehara, K. Toyota, R. Fukuda, J. Hasegawa, M. Ishida, T. Nakajima, Y. Honda, O. Kitao, H. Nakai, T. Vreven, J. A. Montgomery, J. E. Peralta, F. Ogliaro, M. Bearpark, J. J. Heyd, E. Brothers, K. N. Kudin, V. N. Staroverov, R. Kobayashi, J. Normand, K. Raghavachari, A. Rendell, J. C. Burant, S. S. Iyengar, J. Tomasi, M. Cossi, N. Rega, J. M. Millam, M. Klene, J. E. Knox, J. B. Cross, V. Bakken, C. Adamo, J. Jaramillo, R. Gomperts, R. E. Stratmann, O. Yazyev, A. J. Austin, R. Cammi, C. Pomelli, J. W. Ochterski, R. L. Martin, K. Morokuma, V. G. Zakrzewski, G. A. Voth, P. Salvador, J. J. Dannenberg, S. Dapprich, A. D. Daniels, O. Farkas, J. B. Foresman, J. V. Ortiz, J. Cioslowski and D. J. Fox, *Gaussian 09*, Gaussian, Inc., Wallingford CT, 2009.

47 J. Chai and M. Head-Gordon, *Phys. Chem. Chem. Phys.*, 2008, **10**, 6615–6620.

48 R. R. Gagne, C. A. Koval and G. C. Lisensky, *Inorg. Chem.*, 1980, **19**, 2854–2855.

49 Y. Li, J. Wang, X. Zhang, W. Guo, F. Li, M. Yu, X. Kong, W. Wu and Z. Hong, *Org. Biomol. Chem.*, 2015, **13**, 7681–7694.

50 M. L. Agazzi, J. E. Durantini, E. D. Quiroga, M. G. Alvarez and E. N. Durantini, *Photochem. Photobiol. Sci.*, 2021, **20**, 327–341.

51 G. C. Santos, Y. G. Kappenberg, J. M. L. Rosa, A. Ketzer, I. Tisoco, M. A. P. Martins, N. Zanatta, C. P. Frizzo, B. A. Iglesias and H. G. Bonacorso, *J. Photochem. Photobiol., A*, 2023, **444**, 114900.